Ccdc38 is required for sperm flagellum biogenesis and male fertility in mice

Ruidan Zhang[1,2,3#], Bingbing Wu[1,2,3#], Chao Liu[1,2], Zhe Zhang[4,5,6,7], Xiuge Wang[1,3], Liying Wang[1,2], Sai Xiao[1,3], Yinghong Chen[1,3], Huafang Wei[1,2], Hui Jiang[4,5,6,7*], Fei Gao[1,3*], Li Yuan[8*], Wei Li[1,2*]

[1] State Key Laboratory of Stem Cell and Reproductive Biology, Institute of Zoology, Chinese Academy of Sciences, Beijing 100101, China

[2] Institute of Reproductive Health and Perinatology, Guangzhou Women and Children's Medical Center, Guangzhou Medical University, Guangzhou 510623, China

[3] University of the Chinese Academy of Sciences, Beijing 100049, China

[4] Department of Urology, Peking University Third Hospital, Beijing 100191, China

[5] Department of Andrology, Peking University Third Hospital, Beijing 100191, China

[6] Department of Reproductive Medicine Center, Peking University Third Hospital, Beijing 100191, China

[7] Department of Human Sperm Bank, Peking University Third Hospital, Beijing 100191, China

[8] Savaid Medical School, University of Chinese Academy of Sciences, Beijing 100049, China

[#] These authors contributed equally to this work.

*To whom correspondence should be addressed:

Dr. Wei Li

Institute of Reproductive Health and Perinatology,

Guangzhou Women and Children's Medical Center,

Guangzhou Medical University, Guangzhou 510623, China

Tel: +86-10-18910473820,

E-mail: **leways@lzu.edu.cn**

Dr. Li Yuan

Savaid Medical School,

University of Chinese Academy of Sciences

Tel: +86-10-88256717,

E-mail: **yuanli@ucas.ac.cn**

Dr. Fei Gao

Institute of Zoology, Chinese Academy of Sciences,

1-Beichen West Road, Chaoyang District,

Beijing, 100101, China

Tel: +86-10-64807593

E-mail: **gaof@ioz.ac.cn**

Dr. Hui Jiang

Department of Urology; Department of Andrology;

Department of Reproductive Medicine Center;

Department of Human Sperm Bank,

Peking University Third Hospital, Beijing 100191, China

E-mail: **jianghui55@163.com**

Summary statement

CCDC38 participates in manchette assembly and flagellum biogenesis, its defects might be associated with MMAF.

Abstract

The sperm flagellum is essential for male fertility, and defects in flagellum biogenesis are associated with male infertility. Deficiency of CCDC42 is specifically associated with malformation of mouse sperm flagella. Here, we find that the testis-specific expressed protein CCDC38 (coiled-coil domain containing 38) interacts with CCDC42, localizing on the manchette and sperm tail during spermiogenesis. Inactivation of CCDC38 in male mice results in distorted manchette, multiple morphological abnormalities of the flagella (MMAF) of spermatozoa, and eventually male sterility. Furthermore, we find that CCDC38 interacts with intra-flagellar transport protein 88 (IFT88), as well as outer dense fibrous 2 (ODF2), and the knockout of *Ccdc38* reduces transport of ODF2 to the flagellum. Altogether, our results uncover the essential role of CCDC38 in sperm flagellum biogenesis, and suggest that some defects of these genes might be associated with male infertility in humans.

Keywords: MMAF; CCDC38; IFT88; ODF2; Flagellum biogenesis

Introduction

The sperm flagellum is essential for sperm motility (Freitas et al., 2017, Pereira et al., 2017), which is a fundamental requirement for male fertility. The flagellum contains four parts: connecting piece, midpiece, principal piece, and end piece. The core of the sperm flagellum is the central axoneme, which consists of a central microtubule pair (CP) connected to 9 peripheral outer microtubule doublets (MD) to form a '9+2' structure (Sironen et al., 2020). The axoneme possesses radial spokes that connect the central and peripheral microtubules and are related to the mechanical movement of the flagellum (Inaba, 2011). Besides the axoneme, the sperm flagellum contains unique structures, the outer dense fibers (ODFs) and the fibrous sheath (FS), that are not present in cilia or unicellular flagella (Fawcett, 1975). The ODFs are the main cytoskeletal elements of sperm flagella, which are required for sperm motility (Inaba,

2011). ODFs contain 9 fibers in the midpiece, each of which is associated with a microtubule doublet. In humans, ODFs 3 and 8 in the principle piece are replaced by two longitudinal columns of FS, with diminished 3 and 8 fibers ending at the annulus (Azizi and Ghafouri-Fard, 2017, Kim et al., 1999). There are at least 14 polypeptides of ODFs such as ODF1 and ODF2 (Lehti and Sironen, 2017). Any defects in the axoneme structure can cause abnormalities in the sperm flagellum by changing the morphology and causing severe sperm motility disorders (Sha et al., 2014). Thus, axoneme structures are very important to sperm morphology and the function of the flagellum.

Multiple morphological abnormalities of the flagella (MMAF) is a kind of severe teratozoospermia (Coutton et al., 2015), which is characterized by various spermatozoa phenotypes with absent, short, coiled, or irregular flagellum. Many flagellar axoneme defects exist in individuals with MMAF, including disrupted microtubule doublets (MD), ODFs, FSs, outer or inner dynein arms (ODA, IDA) and others (Jiao et al., 2021). Over the past several years, many mutations have been found to be associated with MMAF individuals, and many mouse models display MMAF-like phenotypes, such as *Dnah2* (Li et al., 2019), *Dnah8* (Liu et al., 2020), *Cfap44*, *Cfap65* (Tang et al., 2017, Li et al., 2020), *Qrich2* (Shen et al., 2019), *Cep135* (Sha et al., 2017) and *Ttc21a* (Liu et al., 2019), All are reported as MMAF-related genes. Despite rapid progress made with understanding the mechanism of MMAF, the pathogenesis associated with human idiopathic MMAF remains unknown.

Coiled-coil domain-containing (CCDC) proteins are involved in a variety of physiological and pathological processes. An increasing number of CCDC proteins have been suggested to be involved in ciliogenesis (Priyanka and Yenugu, 2021), yet only some of those genes are involved in spermatogenesis, such as *Ccdc9*, *Ccdc11*, *Ccdc33*, *Ccdc42*, *Ccdc63*, *and Ccdc172*. These genes are associated with sperm flagellum biogenesis and manchette formation, and their defects lead to male

infertility (Sha et al., 2019, Wu et al., 2021, Tapia Contreras and Hoyer-Fender, 2019, Young et al., 2015, Yamaguchi et al., 2014). CCDC42 is a highly expressed protein in mouse testis, which localizes to the manchette, head-to-tail coupling apparatus (HTCA) and sperm tail during spermatogenesis. The protein is necessary for HTCA assembly and sperm flagellum biogenesis (Tapia Contreras and Hoyer-Fender, 2019); however, the functional role of CCDC42 in spermatogenesis is still poorly understood.

Here, we find that CCDC38 interacts with CCDC42, is highly expressed in the testis, and associates with the manchette in the elongating spermatid. Importantly, *Ccdc38* knockout in mice resulted in an abnormally elongated manchette and an MMAF-like phenotype. Furthermore, we find that CCDC38 interacts with IFT88 and ODF2 to facilitate ODF2 transport in the flagella. Our results suggest that the CCDC42-CCDC38 interaction mediates ODF2 transport during flagellum biogenesis, and both proteins are essential for flagellum biogenesis and fertility in mail mice, suggesting mutations of these two genes might be associated with male infertility in humans.

Results

CCDC38 interacts with CCDC42

Many CCDC proteins participate in flagellum biogenesis during spermiogenesis (Priyanka and Yenugu, 2021). CCDC42 localizes to the centrosome, HTCA, manchette and sperm tail in male germ cells, and the protein is involved in the biogenesis of motile cilia and flagellum in mice (Perles et al., 2012, Tapia Contreras and Hoyer-Fender, 2019, Pasek et al., 2016, Silva et al., 2016). To understand the underlying mechanism of CCDC42 in flagellum biogenesis during spermiogenesis, we used the STRING database to search for CCDC42-binding candidates (Fig. 1A). CCDC38, exclusively expressed in testes as reported (Lin et al., 2016), was chosen first. Epitope-tagged CCDC42 and CCDC38 expressed in HEK293T cells followed

by immunoprecipitation experiments demonstrated that CCDC38 was detected in anti-MYC immunoprecipitates from CCDC42 co-transfectants, but not from cells co-transfected with a control plasmid (Fig. 1B). An overlapping immunostaining pattern was clearly found in Hela cells transiently expressing GFP-CCDC38 and MYC-CCDC42, and GFP-CCDC38 could also co-localize with γ-TUBULIN as reported (Firat-Karalar et al., 2014) (Fig. 1C, Fig. S1). These results suggest that CCDC42 can indeed interact with CCDC38.

Next, we examined the localization of endogenous CCDC38 during spermatogenesis. CCDC38 was detected as two adjacent spots near the nuclei of spermatocytes or round spermatids, while it localized to the skirt-like structure encircling the spermatid head from step 9 to step 14 and the testicular sperm tail (Fig. 1D). We, therefore, speculate that CCDC38 might participate in flagellum biogenesis during spermiogenesis.

Ccdc38 knockout leads to male infertility

Reverse transcription-polymerase chain reaction (RT-PCR) revealed that *Ccdc38* could be detected in the testis and was first expressed at postnatal day 14 (P14), peaking on P35 (Fig. 2A, B). To determine the physiological role of CCDC38, we generated *Ccdc38*-deficient mice using the CRISPR/Cas9 system to delete Exon 5 to Exon 11 of the *Ccdc38* gene (Fig. 2C). The *Ccdc38* knockout mice were genotyped by genomic DNA sequencing and further confirmed by PCR, which showed 591 bp for wildtype allele, 750 bp for homozygotes, and two bands of 750bp and 591bp for heterozygotes (Fig. 2D). Subsequent western blotting analysis validated complete ablation of CCDC38 in protein extracted from *Ccdc38*$^{-/-}$ testes (Fig. 2E). We next examined the fertility of *Ccdc38*$^{+/+}$, *Ccdc38*$^{+/-}$, and *Ccdc38*$^{-/-}$ mice. Male *Ccdc38*$^{-/-}$ mice exhibited normal mounting behaviors and produced coital plugs but failed to produce any offspring after mating with WT adult female mice (Fig. 2F). In contrast, female *Ccdc38*$^{-/-}$ mice could generate offspring after mating with WT adult males,

which was similar to that of the *Ccdc38*$^{+/+}$ female mice (Fig. 2G). But the knockout of *Ccdc38* did not affect either testis size (Fig 2H) or the ratio of testis weight and body weight (Fig. 2I, J, K). Taken together, *Ccdc38* knockout leads to male infertility.

Ccdc38 knockout results in MMAF

To further explore the cause of male infertility, we examined the cauda epididymis of *Ccdc38*$^{+/+}$, *Ccdc38*$^{+/-}$, and *Ccdc38*$^{-/-}$ mice by Hematoxylin and Eosin (H&E) staining, and found fewer spermatozoa in the epididymal lumen of *Ccdc38*$^{-/-}$ mice compared with *Ccdc38*$^{+/+}$ and *Ccdc38*$^{+/-}$ mice (Fig. 3A). We next released spermatozoa from the epididymis and found that the number of sperm from *Ccdc38*$^{-/-}$ mice was significantly less than that of *Ccdc38*$^{+/+}$ and *Ccdc38*$^{+/-}$ mice (Fig. 3B). Motile spermatozoa decreased sharply (Fig. 3C), but sperm number and motility showed no obvious differences between *Ccdc38*$^{+/+}$ and *Ccdc38*$^{+/-}$ mice (Fig. 3B, C), thus we focused our attention on *Ccdc38*$^{+/+}$ and *Ccdc38*$^{-/-}$ in subsequent studies. We also noticed that *Ccdc38*$^{-/-}$ spermatozoa showed morphological aberrations, including abnormal nuclei and an MMAF-like phenotype of either short tail (Type 1), disordered filaments (Type 2), impaired spermatozoa head (Type 3), curly tail (Type 4) and tailless (Type 5) (Fig. 3D). The ratio of spermatozoa with abnormal heads and flagella was shown in Fig. 3E. Scanning electron microscopy (SEM) detailed morphological abnormalities of *Ccdc38*$^{-/-}$ spermatozoa as follows (Fig. 3F): short tail (Type 1), disordered filaments (Type 2), impaired spermatozoa head (Type 3), curly tail (Type 4). Therefore, the knockout of *Ccdc38* results in an MMAF-like phenotype in mice.

Spermiogenesis is impaired in *Ccdc38*$^{-/-}$ mice

To further investigate why *Ccdc38* knockout leads to an MMAF-like phenotype, we first used Periodic Acid Schiff (PAS) staining to determine which stages the defects occur. In *Ccdc38*$^{+/+}$ mice testis sections, round spermatids differentiated into elongating spermatids from stage IX, while abnormal elongated spermatids occurred

at stage X in *Ccdc38*$^{-/-}$ mice testis (Fig. 4A). To delineate the detailed defects of *Ccdc38*$^{-/-}$ spermatids, we analyzed steps 1-16 of both *Ccdc38*$^{+/+}$ and *Ccdc38*$^{-/-}$ mice and found that at steps 1-8, the morphology of acrosomes and nuclei of *Ccdc38*$^{-/-}$ spermatids were similar to those of *Ccdc38*$^{+/+}$. In *Ccdc38*$^{+/+}$ mice, spermatid head elongation and maturation began at step 9, while in *Ccdc38*$^{-/-}$ mice, spermatid head elongation and maturation showed abnormalities at step 9, eventually leading to abnormal spermatozoa at step16 (Fig. 4B). These results support that CCDC38 plays an essential role during spermiogenesis.

The flagellum is disorganized and the manchette is ectopically placed in *Ccdc38*$^{-/-}$ spermatids

To study the causes of abnormal sperm morphology after *Ccdc38* depletion, H&E staining was used to detect morphology of seminiferous tubules in *Ccdc38*$^{+/+}$ and *Ccdc38*$^{-/-}$ mice. Compared with *Ccdc38*$^{+/+}$ testis, obvious shortened tails and tailless spermatids could be detected in *Ccdc38*$^{-/-}$ testis (Fig. 5A). Immunofluorescence staining for acetylated TUBULIN (Ac-TUBULIN), the specific flagellum marker, further confirmed the flagellum biogenesis defected in *Ccdc38*$^{-/-}$ testis (Fig. 5B). We conducted immunofluorescence analysis of both PNA and Ac-TUBULIN to determine which stages were affected by *Ccdc38* knockout and found that the flagella of *Ccdc38*$^{-/-}$ spermatids were short and curly from stage IV-V compared with those of *Ccdc38*$^{+/+}$ spermatids (Fig. 5C). By using transmission electron microscopy (TEM), we observed that the outer dense fibers, fibrous sheath, mitochondria sheath and axoneme were also abnormally organized in *Ccdc38*-knockout elongating spermatids (Fig. 5D).

When spermatids were elongated, the sperm head was found to be abnormal, indicating that the manchette might be abnormally formed (Fig. 5C). The manchette is important for sperm head shaping (Wei and Yang, 2018), so we turned our attention to evaluating manchette structure. We found the manchette of *Ccdc38*$^{-/-}$ spermatid

was roughly normal at steps 8-10 but were abnormally longer at steps 11 - 12 compared with the control mice (Fig. 6A). We also used TEM to more fully evaluate manchette and found *Ccdc38*-knockout spermatids, but not control spermatids, became abnormally elongated at step 11 (Fig. 6B). In support of these results, we found that CCDC38 co-localized with α-TUBULIN to manchette in control mice (Fig. 6C). All these results suggest that CCDC38 is directly involved in flagellum biogenesis.

CCDC38 interacts with IFT88

It has been reported that CCDC42, IFT88, CFAP53, and KIF3A are involved in anterograde transport during flagellum biogenesis (Wu et al., 2021). To test whether CCDC38 also participates in anterograde transport by interacting with CFAP53 and IFT complexes, such as IFT88 and IFT20, we co-transfected pCSII-MYC-IFT88, pCSII-MYC-CFAP53 or pRK-FLAG-IFT20 with pEGFP-C1-CCDC38 in HEK293T cells. We next immunoprecipitated CCDC38 with anti-GFP antibody and found that IFT88 and CFAP53, but not IFT20, could be immunoprecipitated by CCDC38 (Fig. 7A-C). We also detected protein expression levels in *Ccdc38*$^{+/+}$ and *Ccdc38*$^{-/-}$ mice testis and found IFT88, CFAP53, and IFT20 expression were all significantly decreased in *Ccdc38*$^{-/-}$ mice testis compared with *Ccdc38*$^{+/+}$ mice testis (Fig. 7D, E). Because IFT88 can participate in anterograde transport, we next evaluated the distribution of IFT88 in spermatids at different steps and found that IFT88 was present in manchette and elongating sperm tails in *Ccdc38*$^{+/+}$ mice, while in the *Ccdc38*$^{-/-}$ spermatids, IFT88 also localized to manchette and elongating sperm tails in spermatids (Fig. 7F). Therefore, CCDC38 might regulate sperm flagellum biogenesis by interacting with IFT88.

ODF transportion is impaired in *Ccdc*38 knockout spermatids

It has been reported that ODF1 and ODF2 can interact with CCDC42 and have been found to be involved in the formation of the male germ cell cytoskeleton (Tapia Contreras and Hoyer-Fender, 2019). To study the relationship between CCDC38 and ODF2, reciprocal co-immunoprecipitation assays were carried out. We transfected pCDNA-HA-ODF2 plasmid and pEGFP-C1-CCDC38 plasmid into HEK293T cells and determined that CCDC38 and ODF2 were able to interact with each other as observed in reciprocal immunoprecipitation experiments (Fig. 8A). These findings suggest that CCDC38 might interact with ODF2.

As the main cytoskeleton protein in ODFs, ODF2 is essential for sperm flagellum integrity and beating (Donkor et al., 2004, Ito et al., 2019, Fawcett, 1975). To determine the effects of *Ccdc38* knockout on ODF1 and ODF2 protein levels, we examined testicular extracts and found that ODF2, but not ODF1, was significantly decreased in *Ccdc38*$^{-/-}$ testicular extracts (Fig. 8B, C) compared with those of *Ccdc38*$^{+/+}$. Next, we used immunofluorescence to detect the expression of ODF2 in spermatids and epididymal spermatozoa. We found that ODF2 localized on the manchette, along with the sperm tail, in elongated spermatids of *Ccdc38*$^{+/+}$ mice, whereas ODF2 was detected on the manchette without tail staining in most of the elongated spermatids of *Ccdc38*$^{-/-}$ mice (Fig. 8D). Of note, ODF2 co-localized with α-TUBULIN on the midpiece and principal piece of *Ccdc38*$^{+/+}$ sperm tails, while ODF2 displayed discontinuous, punctiform signals on only short or curly tails in *Ccdc38*-knockout spermatozoa (Fig. 8E), suggesting that ODF defects in *Ccdc38*-knockout spermatozoa might arise from ODF2 transport defects during spermiogenesis.

Discussion

Ccdc38 is exclusively expressed in testes (Lin et al., 2016), but its role during spermiogenesis has not yet been investigated. To study its role during spermiogenesis, we generated a *Ccdc38*$^{-/-}$ mouse model and found *Ccdc38*$^{-/-}$ male mice to be sterile

(Fig. 2F) due to significantly reduced spermatozoa number and motility (Fig. 3B, C). As for which kinds of cells were affected by CCDC38, a discrepancy exists between our results and others. Lin *et al.* previously reported that CCDC38 is mainly localized to spermatogonia and spermatocytes (Lin et al., 2016), but we found that CCDC38 mainly participates in spermatid elongation and is localized on the manchette and sperm tail (Fig. 1D, 6C). The discrepancy may result from different CCDC38 antibodies being used. Our CCDC38 antibody has been validated by both western blotting (Fig. 2E) and immunofluorescence (Fig. 6C), supporting the robustness of our antibody labeling and the findings of our protein localization in this study. Further support for the manchette and sperm tail protein localization is shown by the knockout of *Ccdc38*, which results in MMAF but dosen't affect ciliogenesis in the lung and trachea of *Ccdc38*$^{-/-}$ mice (Fig. S2). These results suggest that CCDC38 should be directly involved in flagellum biogenesis but not other processes.

The manchette is a transient structure in developing germ cells, which is required for sperm nuclear condensation and flagellum biogenesis (Wei and Yang, 2018) by providing the structural basis for intra-manchette transport (IMT). IMT transfers structural and functional proteins to the basal body and is essential for nucleocytoplasmic transport (Kierszenbaum, 2002, Kierszenbaum et al., 2002). As an IMT component, CCDC42 localizes to the manchette, connecting piece and sperm tail during spermiogenesis, and can interact with ODF1 and ODF2 to regulate germ cell cytoskeleton formation (Tapia Contreras and Hoyer-Fender, 2019, Pasek et al., 2016). In this study, we found that CCDC38 interacts with CCDC42, co-localizes with CCDC42 on centrosomes in Hela cells (Fig. 1A, B, C), and interacts with ODF2 and ODF1 (Fig. 8A, Fig. S3). Both ODF1 and ODF2 are components of ODFs and are very important for male fertility. The knockout of *Odf1* in mice impairs sperm head-to-tail coupling (Yang et al., 2014, Yang et al., 2012), while the knockout of *Odf2* leads to preimplantation lethality. Even the absence of a single copy of this gene results in sperm neck-midpiece separation (Qian et al., 2016, Tarnasky et al., 2010).

Furthermore, recent human infertility studies showed that mutations in *ODF2* caused MMAF (Zhu et al., 2022). Consistent with the clinical studies, we found that once *Ccdc38* was knocked out, ODF2 but not ODF1 protein levels decreased in the testis (Fig. 8B, C) and ODF2 distribution was disturbed in flagella (Fig. 8D, E). Thus, CCDC38 either works as a partner of ODF2 to support its stability or participates in IMT to mediate ODF2 transport during flagellum biogenesis. Since CCDC38 also interacted with CCDC42, we believe CCDC38 plays a role in ODF2 transport, and this is further supported by its interaction with IFT88.

In addition to IMT, intra-flagellar transport is also required for flagellum biogenesis. IFT is responsible for sperm-protein transport during the development of the flagella. During IFT, cargo is transported from the basal body to the tip of the flagellum and then back to the sperm head along the axoneme (Scholey, 2003, Taschner and Lorentzen, 2016, Ishikawa and Marshall, 2017). IFT88 is an IFT B component and is present only in the heads and tails of elongating spermatids, and not in mature sperm (San Agustin et al., 2015). IFT88 has been found to interact with Kinesin to regulate anterograde transport along the axoneme (Rosenbaum and Witman, 2002). Working as an IFT88 interacting protein (Fig. 7A), CCDC38 may also participate in the anterograde transport along the flagellum. Previously, we found that CFAP53 could interact with both CCDC42 and IFT88 to regulate the anterograde transport along the flagellum (Wu et al., 2021). In this study, we found that CCDC38 also interacts with CFAP53 (Fig. 7B). Thus, CCDC38 may interact with CFAP53, CCDC42 and IFT88 to regulate cargo transport by IMT and IFT during flagellum biogenesis. Further investigations are definitely needed to reveal the detailed roles of these proteins and their relationships during flagellum biogenesis.

In summary, we have identified a new CCDC42 interacting protein, CCDC38, that is essential for spermiogenesis and flagellum biogenesis, as the knockout of *Ccdc38* results in an MMAF-like phenotype in mice. Since these genes are evolutionarily conserved in humans, we believe that mutations of these genes may

exist in individuals with MMAF and further studies are needed to be undertaken to uncover how these mutations affect disease presentation.

Materials and methods

Animals

The mouse *Ccdc38* gene is 1692 bp and contains 16 exons. *Ccdc38*-knockout mice were generated using the CRISPER/Cas9 system from Cyagen Biosciences. Genotyping primers for knockout were as follows:

F1: GTAGCTGTTTCTAAGCGATCATCA,

R1: ACTAGGTACCTCAAGCTGGTTTAGA

Genotyping primers for WT mice were as follows:

F1: GTAGCTGTTTCTAAGCGATCATCA,

R2: GTCATGGGACAGATGTGGAACTA.

All animal experiments were performed according to approved institutional animal care and use committee (IACUC) protocols (# 08-133) of the Institute of Zoology, Chinese Academy of Sciences.

Antibodies

Mouse anti-GFP antibody (M20004L, Abmart) and rabbit anti-MYC antibody (BE2011, Abmart) were each used at a dilution of 1:1000 for western blotting. ODF2 antibody (12058-1-AP, Proteintech) was used at a dilution of 1:1000 for western blotting and 1: 200 for immunofluorescence. Mouse anti-α-TUBULIN antibody (AC012, Abclonal) was used at a dilution of 1:100 for immunofluorescence. Mouse anti-α/β-TUBULIN antibody (ab44928, Abcam) was used at a dilution of 1: 100 for immunofluorescence. Mouse anti-GAPDH antibody (AC002, Abclonal) was used at a dilution of 1:10000 for western blotting. Mouse anti-ODF1 antibody (sc-390152, Santa Cruz) was used at a dilution of 1:500 for western blotting. Mouse anti-Ac-TUBULIN antibody (T7451, Sigma-Aldrich) was used at a dilution of 1:200 for

immunofluorescence. Mouse anti-CCDC38 were generated by Dia-an Biotech (Wuhan, China) and was used at a dilution of 1:20 for immunofluorescence. Rabbit anti-CCDC38 were generated by Dia-an Biotech (Wuhan, China) and was used at a dilution of 1:500 for western blotting. The Alexa Fluor 488 conjugate of lectin PNA (1:400, L21409, Thermo Fisher) was used for immunofluorescence. Secondary antibodies were goat anti-rabbit FITC (1:200, ZF-0311, Zhong Shan Jin Qiao), goat anti-TRITC (1:200, ZF-0316, Zhong Shan Jin Qiao), goat anti-mouse FITC (1:200, ZF-0312, Zhong Shan Jin Qiao), and goat anti-rabbit TRITC (1:200, ZF0313, Zhong Shan Jin Qiao).

Immunoblotting

As previously reported (Liu et al., 2016), testis albuginea was peeled and added to RIPA buffer supplemented with 1mM phenyl methyl sulfonyl fluoride (PMSF) and PIC (Roche Diagnostics, 04693132001). The solution was sonicated transiently and then placed on the ice for 30 min. Samples were centrifuged at 12000 rpm for 15 min at 4℃. Next, the supernatant was collected in a new tube. Protein lysates were electrophoresed and electrotransferred to an NC memberane. The membrane was then incubated with primary antibody and a second antibody. Finally, the membrane was scanned via an Odyssey infrared imager (LI-COR Biosciences, Lincoln, NE, RRID: SCR_014579).

Immunoprecipitation

Transfected cells were lysed in a lysis buffer (50mM HEPES, PH 7.4, 250mM NaCl, 0.1% NP-40 containing PIC and PMSF) on ice for 30 min and centrifuged at 12000 rpm at 4℃ for 15 min. Cell lysates were first incubated with primary antibody overnight at 4℃ and then incubated with protein A-Sepharose (GE, 17-1279-03) for 2h at 4℃. The precipitants were washed 3 times with lysis buffer, added the SDS loading buffer, heated for 10 min at 95℃ and subjected to immunoblotting analysis.

Epididymal sperm count

The cauda epididymis was isolated from 8-week old mice. Sperm was released from the cauda epididymis in HTF and incubated at 37℃ for 15 min. The medium was then diluted to 1:100 and sperm were counted with a hemocytometer.

Tissue collection and histological analysis

As previously reported (Wang et al., 2018), the testes were dissected after euthanasia, and fixed with Bouin's fixative for 24h at 4 ℃. Next, the testes were dehydrated with graded ethanol and embedded in paraffin. 5um sections were cut and placed on glass slides. Sections were stained with H&E and PAS for histological analysis after deparaffinization.

Transmission electron microscopy

Testis were processed using methods previously reported, with some modifications (Liu et al., 2016). Briefly, the testis from WT and *Ccdc38*-knockout mice testis and epididymis were dissected and fixed in 2.5% (vol/vol) glutaraldehyde in 0.1 M cacodylate buffer at 4℃ overnight. After washing in 0.1 M cacodylate buffer, samples were cut into small pieces, then immersed in 1% OsO4 for 1h at 4℃. Samples were dehydrated through a graded acetone series (50%, 60%, 70%, 80%, 90%, 95%, 100%) and embedded in resin (DDSA, NMA, enhancer, 812) for staining. Ultrathin sections were cut and stained with uranyl acetate and lead citrate, images were acquired and analyzed using a JEM-1400 transmission electron microscope.

Scanning electron microscopy

Sperm was released from the epididymis in HTF at 37℃ for 15 min, centrifugated 5 min at 500 g, washed twice with PB, and fixed in 2.5% glutaraldehyde solution overnight. Samples were finally dehydrated in graded ethanol, subjected to drying and

coated with gold. Images were acquired and analyzed using a SU8010 scanning electron microscope.

Immunofluorescence

The testis albuginea was peeled and incubated with collagenase IV and hyaluronidase in PBS for 15 min at 37℃, then washed twice with PBS. Next, the sample was fixed with 4% PFA for 5 min, and then coated on a glass slide to dry out. The slides were washed with PBS three times, treated with 0.5% TritonX-100 for 5 min, and finally blocked with 5% BSA for 30 min. A primary antibody was incubated with the sample at 4℃ overnight, followed by a second antibody and DAPI. Images were taken using LSM880 and Sp8 microscopes.

Statistical Analysis

All data are presented as the mean ± SD. Statistical significance of the differences between the mean values for the various genotypes was measured by Student's t-tests with paired, 2-tailed distribution. The data were considered significant when *P*-values were less than 0.05(*), 0.01(**) or 0.001(***).

Acknowledgments

This work was funded by the National Science Fund for Distinguished Young Scholars (81925015), the National Natural Science Foundation of China (91649202) and the Strategic Priority Research Program of the Chinese Academy of Sciences (grant XDA16020701).

Authors Contributions

RDZ and BBW performed most of the experiments and wrote the manuscript. CL, XGW, ZZ, LYW, SX, YHC and HJ performed part of the experiment. WL, YL, FG and HJ supervised the whole project and revised the manuscript.

Compliance with ethical standards

All animal experiments were performed according to approved institutional animal care and use committee (IACUC) protocols (#08-133) of the Institute of Zoology, Chinese Academy of Sciences. All surgery was performed under sodium pentobarbital anesthesia, and every effort was made to minimize suffering.

Conflict of interest

The authors declare that they have no conflict of interest.

References

AZIZI, F. and GHAFOURI-FARD, S. (2017). Outer Dense Fiber Proteins: Bridging between Male Infertility and Cancer. *Arch Iran Med,* **20,** 320-325.

COUTTON, C., ESCOFFIER, J., MARTINEZ, G., ARNOULT, C. and RAY, P. F. (2015). Teratozoospermia: spotlight on the main genetic actors in the human. *Hum Reprod Update,* **21,** 455-85.

DONKOR, F. F., MONNICH, M., CZIRR, E., HOLLEMANN, T. and HOYER-FENDER, S. (2004). Outer dense fibre protein 2 (ODF2) is a self-interacting centrosomal protein with affinity for microtubules. *J Cell Sci,* **117,** 4643-51.

FAWCETT, D. W. (1975). The mammalian spermatozoon. *Dev Biol,* **44,** 394-436.

FIRAT-KARALAR, E. N., SANTE, J., ELLIOTT, S. and STEARNS, T. (2014). Proteomic analysis of mammalian sperm cells identifies new components of the centrosome. *J Cell Sci,* **127,** 4128-33.

FREITAS, M. J., VIJAYARAGHAVAN, S. and FARDILHA, M. (2017). Signaling mechanisms in mammalian sperm motility. *Biol Reprod,* **96,** 2-12.

INABA, K. (2011). Sperm flagella: comparative and phylogenetic perspectives of protein components. *Mol Hum Reprod,* **17,** 524-38.

ISHIKAWA, H. and MARSHALL, W. F. (2017). Intraflagellar Transport and Ciliary Dynamics. *Cold Spring Harb Perspect Biol,* **9**.

ITO, C., AKUTSU, H., YAO, R., YOSHIDA, K., YAMATOYA, K., MUTOH, T., MAKINO, T., AOYAMA, K., ISHIKAWA, H., KUNIMOTO, K., et al. (2019). Odf2 haploinsufficiency causes a new type of decapitated and decaudated spermatozoa, Odf2-DDS, in mice. *Sci Rep,* **9,** 14249.

JIAO, S. Y., YANG, Y. H. and CHEN, S. R. (2021). Molecular genetics of infertility: loss-of-function mutations in humans and corresponding knockout/mutated mice. *Hum Reprod Update,* **27,** 154-189.

KIERSZENBAUM, A. L. (2002). Intramanchette transport (IMT): managing the making of the spermatid head, centrosome, and tail. *Mol Reprod Dev,* **63,** 1-4.

KIERSZENBAUM, A. L., GIL, M., RIVKIN, E. and TRES, L. L. (2002). Ran, a GTP-binding protein involved in nucleocytoplasmic transport and microtubule nucleation, relocates from the manchette to the centrosome region during rat spermiogenesis. *Mol Reprod Dev,* **63,** 131-40.

KIM, Y. H., MCFARLANE, J. R., O'BRYAN, M. K., ALMAHBOBI, G., TEMPLE-SMITH, P. D. and DE KRETSER, D. M. (1999). Isolation and characterization of rat sperm tail outer dense fibres and comparison with rabbit and human spermatozoa using a polyclonal antiserum. *J Reprod Fertil,* **116,** 345-53.

LEHTI, M. S. and SIRONEN, A. (2017). Formation and function of sperm tail structures in association with sperm motility defects. *Biol Reprod,* **97,** 522-536.

LI, L., FENG, F., WANG, Y., GUO, J. and YUE, W. (2020). Mutational effect of human CFAP43 splice-site variant causing multiple morphological abnormalities of the sperm flagella. *Andrologia,* **52,** e13575.

LI, Y., SHA, Y., WANG, X., DING, L., LIU, W., JI, Z., MEI, L., HUANG, X., LIN, S., KONG, S., et al. (2019). DNAH2 is a novel candidate gene associated with multiple morphological abnormalities of the sperm flagella. *Clin Genet,* **95,** 590-600.

LIN, S. R., LI, Y. C., LUO, M. L., GUO, H., WANG, T. T., CHEN, J. B., MA, Q., GU, Y. L., JIANG, Z. M. and GUI, Y. T. (2016). Identification and characteristics of the testes-specific gene, Ccdc38, in mice. *Mol Med Rep,* **14,** 1290-6.

LIU, C., MIYATA, H., GAO, Y., SHA, Y., TANG, S., XU, Z., WHITFIELD, M., PATRAT, C., WU, H., DULIOUST, E., et al. (2020). Bi-allelic DNAH8 Variants Lead to Multiple Morphological Abnormalities of the Sperm Flagella and Primary Male Infertility. *Am J Hum Genet,* **107,** 330-341.

LIU, C., WANG, H., SHANG, Y., LIU, W., SONG, Z., ZHAO, H., WANG, L., JIA, P., GAO, F., XU, Z., et al. (2016). Autophagy is required for ectoplasmic specialization assembly in sertoli cells. *Autophagy,* **12,** 814-32.

LIU, W., HE, X., YANG, S., ZOUARI, R., WANG, J., WU, H., KHERRAF, Z. E., LIU, C., COUTTON, C., ZHAO, R., et al. (2019). Bi-allelic Mutations in TTC21A Induce Asthenoteratospermia in Humans and Mice. *Am J Hum Genet,* **104,** 738-748.

PASEK, R. C., MALARKEY, E., BERBARI, N. F., SHARMA, N., KESTERSON, R. A., TRES, L. L., KIERSZENBAUM, A. L. and YODER, B. K. (2016). Coiled-coil domain containing 42 (Ccdc42) is necessary for proper sperm development and male fertility in the mouse. *Dev Biol,* **412,** 208-18.

PEREIRA, R., SA, R., BARROS, A. and SOUSA, M. (2017). Major regulatory mechanisms involved in sperm motility. *Asian J Androl,* **19,** 5-14.

PERLES, Z., CINNAMON, Y., TA-SHMA, A., SHAAG, A., EINBINDER, T., REIN, A. J. and ELPELEG, O. (2012). A human laterality disorder associated with recessive CCDC11 mutation. *J Med Genet,* **49,** 386-90.

PRIYANKA, P. P. and YENUGU, S. (2021). Coiled-Coil Domain-Containing (CCDC) Proteins: Functional Roles in General and Male Reproductive Physiology. *Reprod Sci*.

QIAN, X., WANG, L., ZHENG, B., SHI, Z. M., GE, X., JIANG, C. F., QIAN, Y. C., LI, D. M., LI, W., LIU, X., et al. (2016). Deficiency of Mkrn2 causes abnormal spermiogenesis and spermiation, and impairs male fertility. *Sci Rep,* **6,** 39318.

ROSENBAUM, J. L. and WITMAN, G. B. (2002). Intraflagellar transport. *Nat Rev Mol Cell Biol,* **3,** 813-25.

SAN AGUSTIN, J. T., PAZOUR, G. J. and WITMAN, G. B. (2015). Intraflagellar transport is essential for mammalian spermiogenesis but is absent in mature sperm. *Mol Biol Cell,* **26,** 4358-72.

SCHOLEY, J. M. (2003). Intraflagellar transport. *Annu Rev Cell Dev Biol,* **19,** 423-43.

SHA, Y.-W., XU, X., MEI, L.-B., LI, P., SU, Z.-Y., HE, X.-Q. and LI, L. (2017). A homozygous CEP135 mutation is associated with multiple morphological abnormalities of the sperm flagella (MMAF). *Gene,* **633,** 48-53.

SHA, Y., XU, Y., WEI, X., LIU, W., MEI, L., LIN, S., JI, Z., WANG, X., SU, Z., QIU, P., et al. (2019). CCDC9 is identified as a novel candidate gene of severe asthenozoospermia. *Syst Biol Reprod Med,* **65,** 465-473.

SHA, Y. W., DING, L. and LI, P. (2014). Management of primary ciliary dyskinesia/Kartagener's syndrome in infertile male patients and current progress in defining the underlying genetic mechanism. *Asian J Androl,* **16,** 101-6.

SHEN, Y., ZHANG, F., LI, F., JIANG, X., YANG, Y., LI, X., LI, W., WANG, X., CHENG, J., LIU, M., et al. (2019). Loss-of-function mutations in QRICH2 cause male infertility with multiple morphological abnormalities of the sperm flagella. *Nat Commun,* **10,** 433.

SILVA, E., BETLEJA, E., JOHN, E., SPEAR, P., MORESCO, J. J., ZHANG, S., YATES, J. R., 3RD, MITCHELL, B. J. and MAHJOUB, M. R. (2016). Ccdc11 is a novel centriolar satellite protein essential for ciliogenesis and establishment of left-right asymmetry. *Mol Biol Cell,* **27,** 48-63.

SIRONEN, A., SHOEMARK, A., PATEL, M., LOEBINGER, M. R. and MITCHISON, H. M. (2020). Sperm defects in primary ciliary dyskinesia and related causes of male infertility. *Cell Mol Life Sci,* **77,** 2029-2048.

TANG, S., WANG, X., LI, W., YANG, X., LI, Z., LIU, W., LI, C., ZHU, Z., WANG, L., WANG, J., et al. (2017). Biallelic Mutations in CFAP43 and CFAP44 Cause Male Infertility with Multiple Morphological Abnormalities of the Sperm Flagella. *Am J Hum Genet,* **100,** 854-864.

TAPIA CONTRERAS, C. and HOYER-FENDER, S. (2019). CCDC42 Localizes to Manchette, HTCA and Tail and Interacts With ODF1 and ODF2 in the Formation of the Male Germ Cell Cytoskeleton. *Front Cell Dev Biol,* **7,** 151.

TARNASKY, H., CHENG, M., OU, Y., THUNDATHIL, J. C., OKO, R. and VAN DER HOORN, F. A. (2010). Gene trap mutation of murine outer dense fiber protein-2 gene can result in sperm tail abnormalities in mice with high percentage chimaerism. *BMC Dev Biol,* **10,** 67.

TASCHNER, M. and LORENTZEN, E. (2016). The Intraflagellar Transport Machinery. *Cold Spring Harb Perspect Biol,* **8**.

WANG, L., TU, Z., LIU, C., LIU, H., KALDIS, P., CHEN, Z. and LI, W. (2018). Dual roles of TRF1 in tethering telomeres to the nuclear envelope and protecting them from fusion during meiosis. *Cell Death Differ,* **25,** 1174-1188.

WEI, Y. L. and YANG, W. X. (2018). The acroframosome-acroplaxome-manchette axis may function in sperm head shaping and male fertility. *Gene,* **660,** 28-40.

WU, B., YU, X., LIU, C., WANG, L., HUANG, T., LU, G., CHEN, Z. J., LI, W. and LIU, H. (2021). Essential Role of CFAP53 in Sperm Flagellum Biogenesis. *Front Cell Dev Biol,* **9,** 676910.

YAMAGUCHI, A., KANEKO, T., INAI, T. and IIDA, H. (2014). Molecular cloning and subcellular localization of Tektin2-binding protein 1 (Ccdc 172) in rat spermatozoa. *J Histochem Cytochem,* **62,** 286-97.

YANG, K., GRZMIL, P., MEINHARDT, A. and HOYER-FENDER, S. (2014). Haplo-deficiency of ODF1/HSPB10 in mouse sperm causes relaxation of head-to-tail linkage. *Reproduction,* **148,** 499-506.

YANG, K., MEINHARDT, A., ZHANG, B., GRZMIL, P., ADHAM, I. M. and HOYER-FENDER, S. (2012). The small heat shock protein ODF1/HSPB10 is essential for tight linkage of sperm head to tail and male fertility in mice. *Mol Cell Biol,* **32,** 216-25.

YOUNG, S. A., MIYATA, H., SATOUH, Y., KATO, H., NOZAWA, K., ISOTANI, A., AITKEN, R. J., BAKER, M. A. and IKAWA, M. (2015). CRISPR/Cas9-Mediated Rapid Generation of Multiple Mouse Lines Identified Ccdc63 as Essential for Spermiogenesis. *Int J Mol Sci,* **16,** 24732-50.

ZHU, Z. J., WANG, Y. Z., WANG, X. B., YAO, C. C., ZHAO, L. Y., ZHANG, Z. B., WU, Y., CHEN, W. and LI, Z. (2022). Novel mutation in ODF2 causes multiple morphological abnormalities of the sperm flagella in an infertile male. LID - 10.4103/aja202183 [doi].

Figures

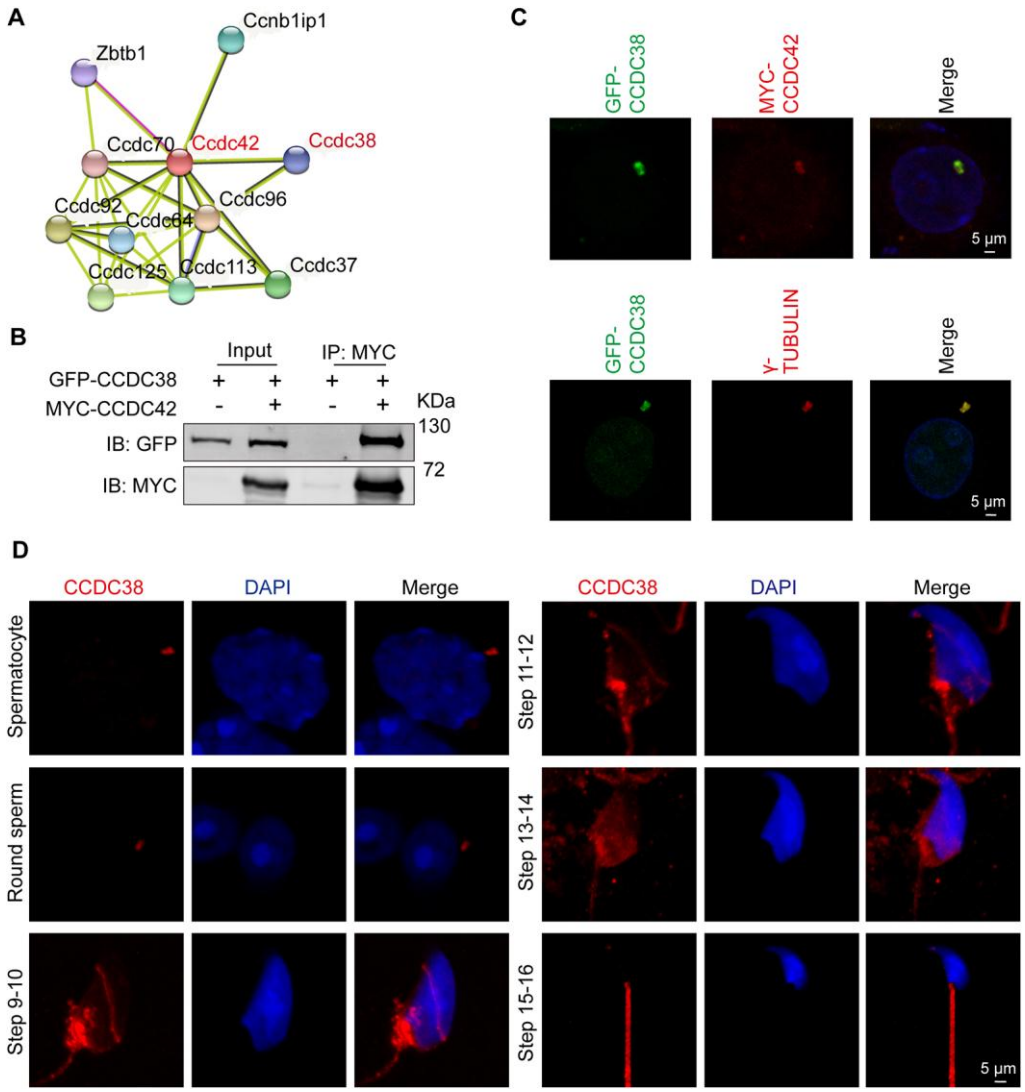

Fig. 1. CCDC38 interacts with CCDC42. (A) CCDC38 might interact with CCDC42 as predicted by the STRING database. (B) CCDC38 interacted with CCDC42. pCSII-MYC-CCDC42 and pEGFP-C1-CCDC38 plasmids were transfected into HEK293T cells. Forty-eight hours after transfection, cells were collected for immunoprecipitation with anti-MYC antibody, and detected by anti-MYC antibodies or anti-GFP, respectively. (C) CCDC38 co-localized with CCDC42 and γ-TUBULIN in Hela cells. pCSII-MYC-CCDC42 and pEGFP-C1-CCDC38 plasmids were co-transfected into Hela cells. Forty-eight hours after transfection, cells were fixed and

stained with anti-MYC and γ-TUBULIN antibodies, and the nuclei were stained with DAPI. (D) Testicular germ cells were stained with anti-CCDC38 antibody, and the nuclei were stained with DAPI. Scale bars: 5 μm.

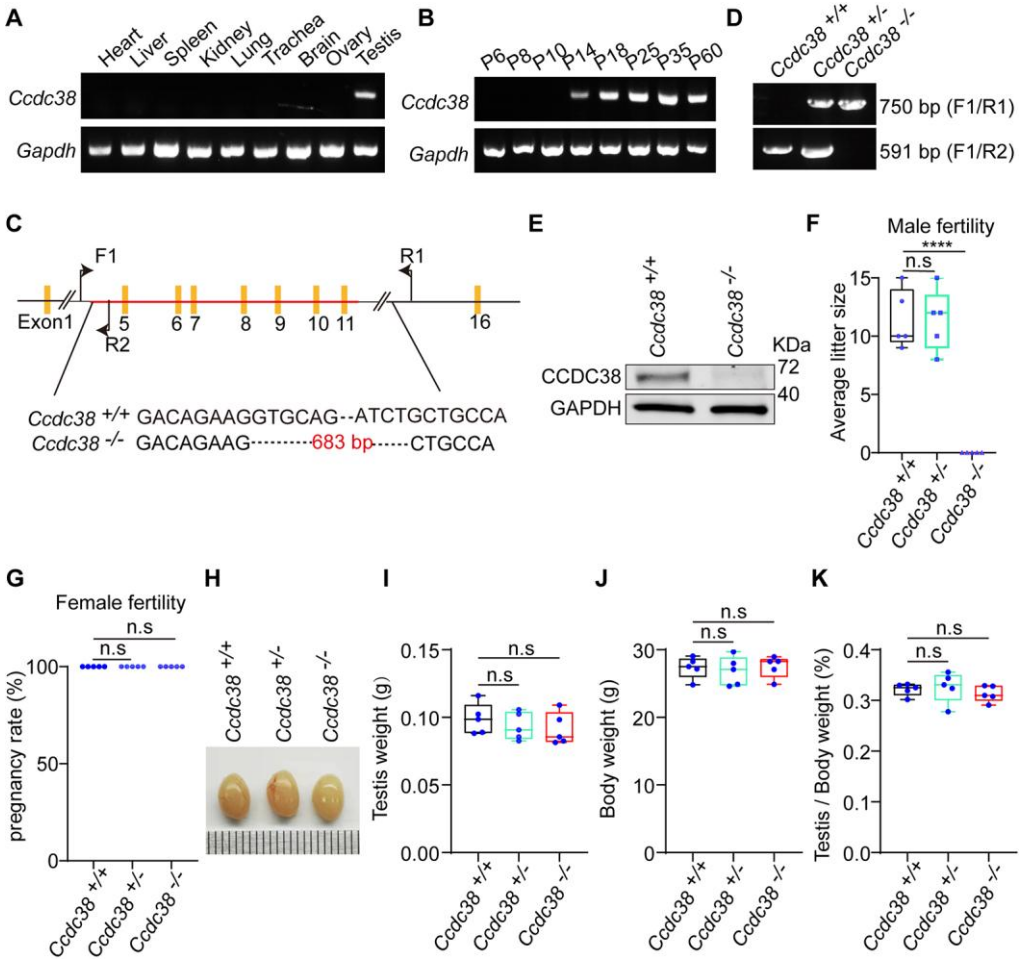

Fig. 2. *Ccdc38* knockout leads to male infertility. (A) The expression of *Ccdc38* in different tissues. (B) Expression of *Ccdc38* on different days. (C) Generation of *Ccdc38*$^{-/-}$ mice lacking exon 5-11. (D) Genotyping of *Ccdc38*$^{+/+}$, *Ccdc38*$^{+/-}$, and *Ccdc38*$^{-/-}$ mice. (E) Western blot of CCDC38 to show the depletion efficiency of *Ccdc38*$^{-/-}$ male mice. (F) The average litter size of *Ccdc38*$^{+/+}$, *Ccdc38*$^{+/-}$, and *Ccdc38*$^{-/-}$ mice at 2 months. No pregnancy occurred in females mated with *Ccdc38*$^{-/-}$ male mice. ****$P < 0.0001$. (G) Pregnancy rate of *Ccdc38*$^{+/+}$, *Ccdc38*$^{+/-}$, and *Ccdc38*$^{-/-}$ female mice at 2 months. No obvious difference was observed between *Ccdc38*$^{+/+}$, *Ccdc38*$^{+/-}$, and *Ccdc38*$^{-/-}$ mice. (H) The size of the *Ccdc38*$^{+/+}$, *Ccdc38*$^{+/-}$, and *Ccdc38*$^{-/-}$ mice testes were not affected. (I) Testis from *Ccdc38*$^{+/+}$, *Ccdc38*$^{+/-}$, and *Ccdc38*$^{-/-}$ male mice had no obvious difference in weight (n=5). (J) Body weight of *Ccdc38*$^{+/+}$,

Ccdc38$^{+/-}$, and *Ccdc38*$^{-/-}$ male mice showed no obvious difference (n=5). (K) Ratios of testis/body weight in *Ccdc38*$^{+/+}$, *Ccdc38*$^{+/-}$, and *Ccdc38*$^{-/-}$ male mice were consistent (n=5). Data are presented as the mean ± SD.

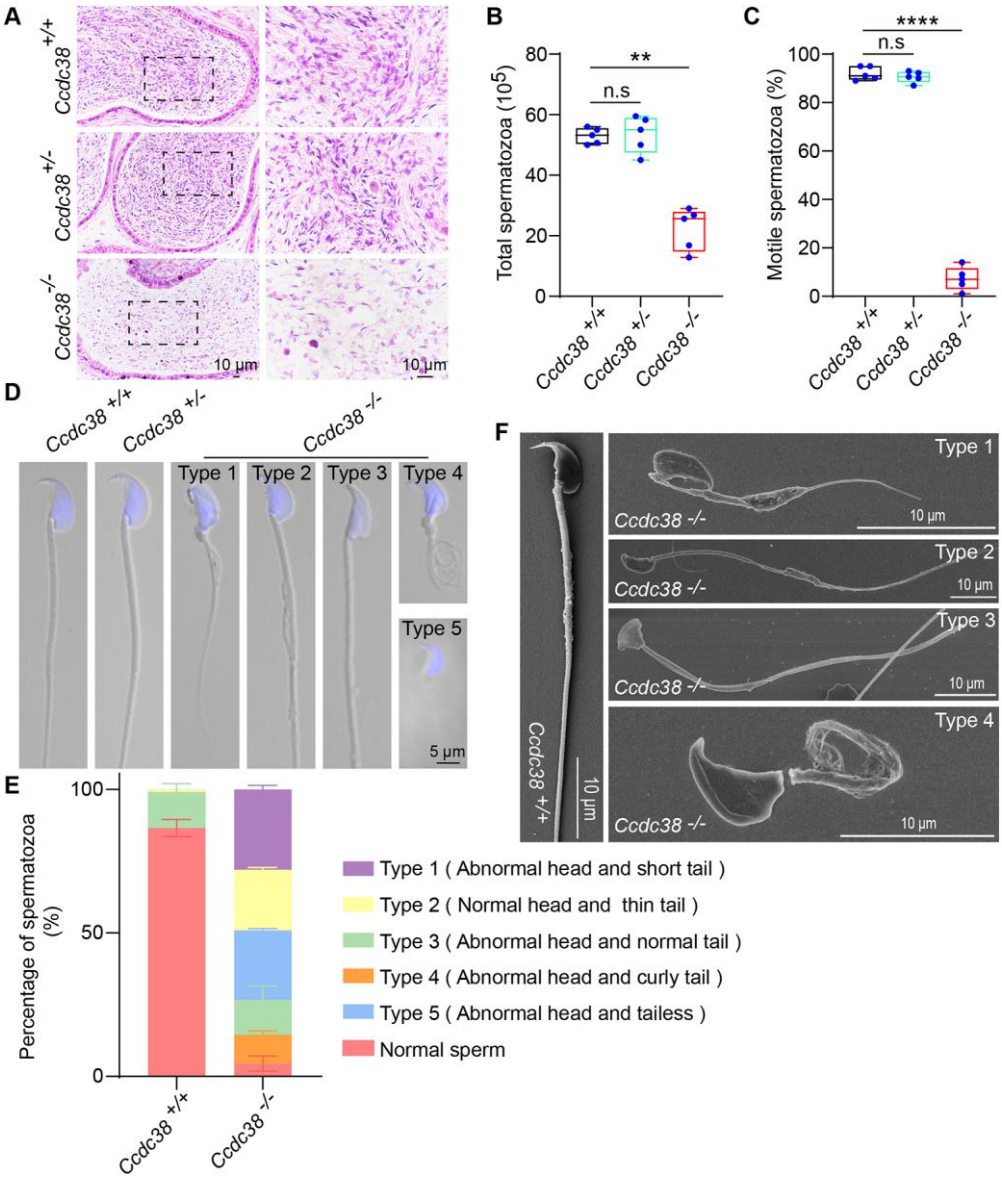

Fig. 3. *Ccdc38* knockout results in MMAF. (A) H&E staining of the caudal epididymis. (B) Sperm number obtained from *Ccdc38*$^{+/+}$, *Ccdc38*$^{+/-}$, and *Ccdc38*$^{-/-}$ mice (n=5), $^{**}P < 0.01$. (C) The ratio of motile spermatozoa from *Ccdc38*$^{+/+}$, *Ccdc38*$^{+/-}$, and *Ccdc38*$^{-/-}$ mice (n=5), $^{****}P < 0.0001$. (D) With single-sperm immunofluorescence analysis of *Ccdc38*$^{+/+}$, *Ccdc38*$^{+/-}$, and *Ccdc38*$^{-/-}$ mice, the nucleus was stained with DAPI and 5 sperm phenotypes were observed: short tail, disordered tail, abnormal nuclei, curly tail and tailless. (E) The percentage of different spermatozoa observed in *Ccdc38*$^{+/+}$ and *Ccdc38*$^{-/-}$ caudal epididymis. (F) Scanning

electron microscopy analysis of spermatozoa from the epididymis of *Ccdc38*$^{+/+}$ and *Ccdc38*$^{-/-}$ mice. A similar morphology was seen in the SEM analysis except for the tailless spermatozoa. Data are presented as the mean ± SD. Scale bars: 10 μm (A, E); 5 μm (D).

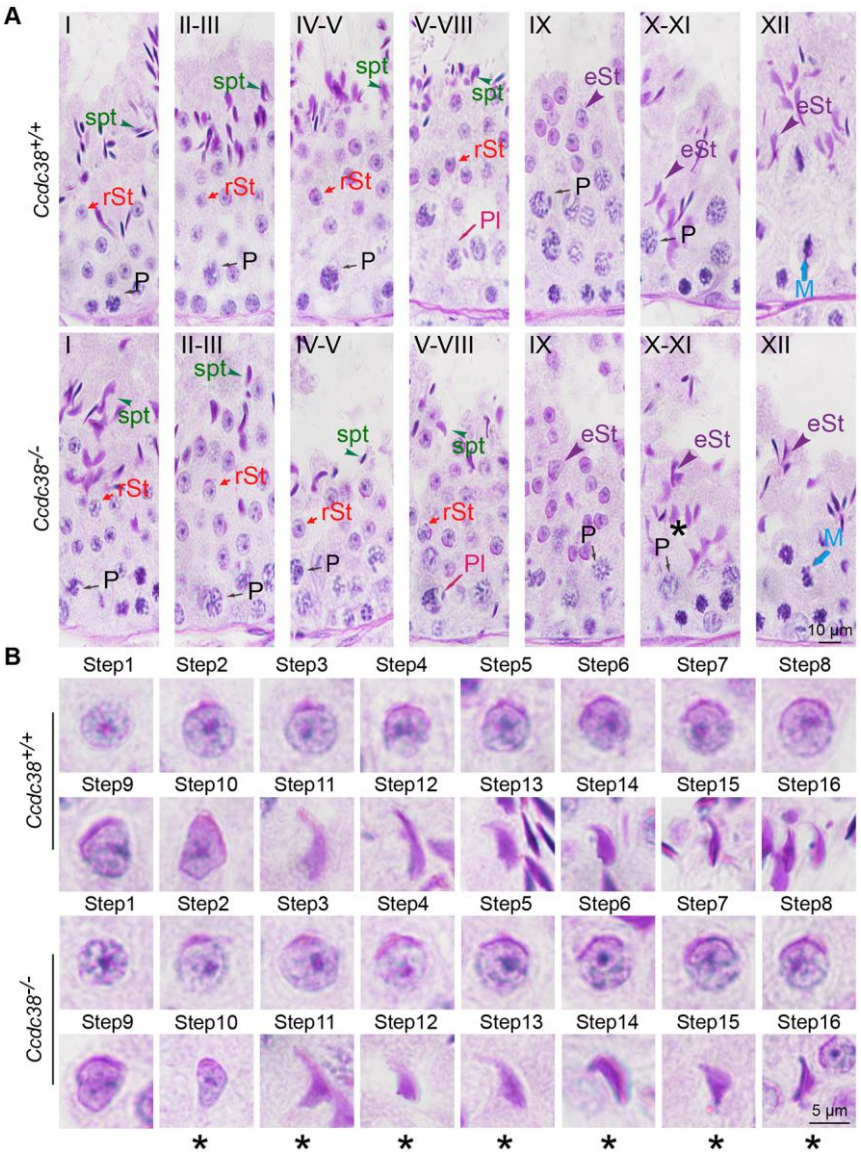

Fig. 4. Spermiogenesis is impaired in *Ccdc38*$^{-/-}$ mice. (A) PAS staining of *Ccdc38*$^{-/-}$ testis sections showed abnormal sperm nuclear shape. P: pachytene, rSt: round spermatid, spt: spermatozoa, M: meiotic spermatocyte, eSt: elongating spermatid. The asterisk indicates abnormal elongated spermatid at stage X-XI in *Ccdc38*$^{-/-}$ mice. (B) PAS staining of spermatids at different steps from *Ccdc38*$^{+/+}$ and *Ccdc38*$^{-/-}$ mice. Asterisks indicate abnormal spermatid shapes found starting at step 10. Scale bars: 10 μm (A); 5 μm (B).

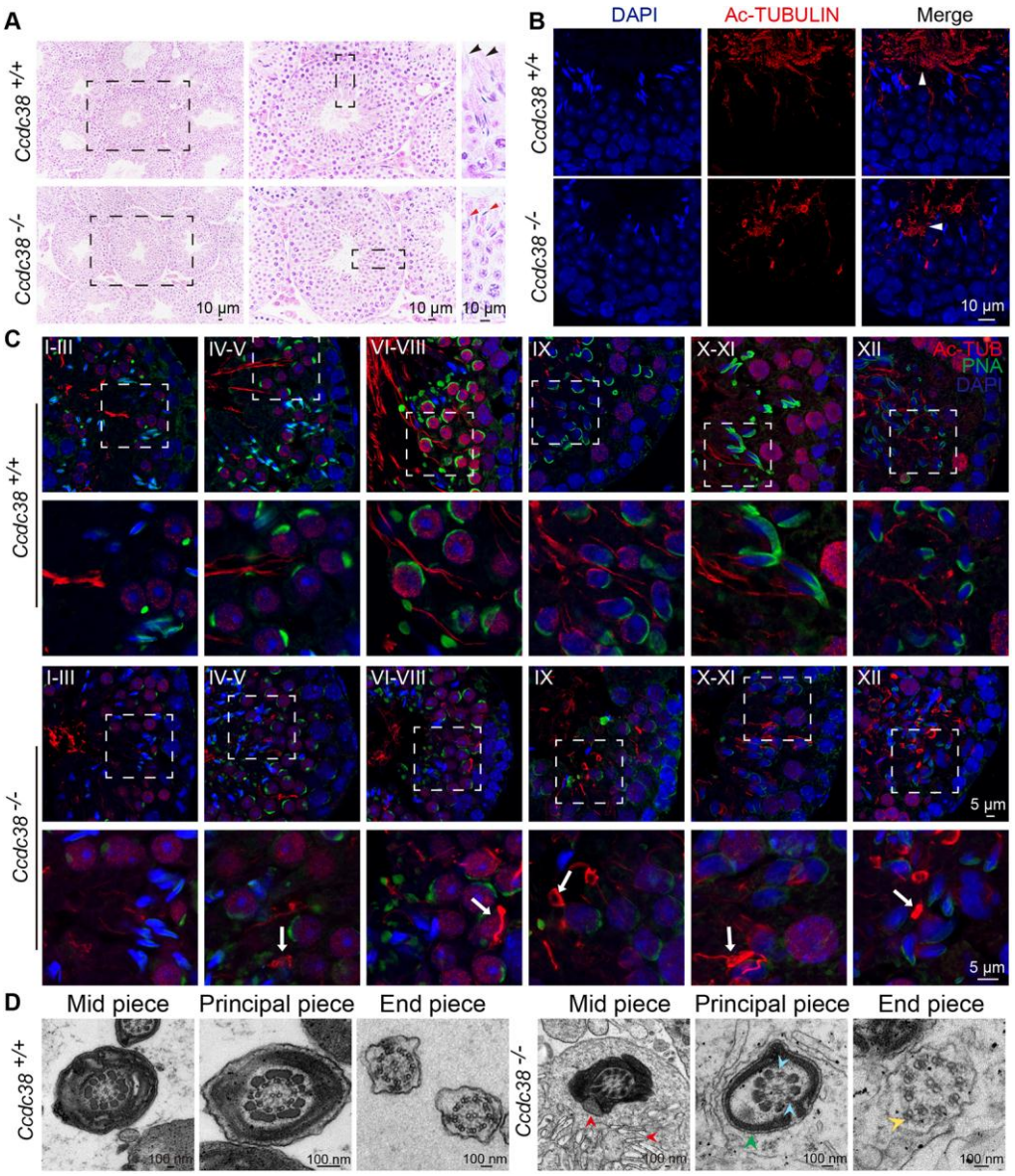

Fig. 5. The flagellum is disorganized in *Ccdc38*$^{-/-}$ spermatids. (A) The histology of the seminiferous tubules from *Ccdc38*$^{+/+}$ and *Ccdc38*$^{-/-}$ male mice. Black arrowheads indicate normal sperm tails in the *Ccdc38*$^{+/+}$ mice testis seminiferous tubule, red arrowheads indicate the abnormal sperm flagellum in the *Ccdc38*$^{-/-}$ mice testis seminiferous tubule. (B) Immunofluorescence analysis of Ac-TUBULIN (red) antibodies in *Ccdc38*$^{-/-}$ mice testes showed flagellar defects. The nucleus was stained with DAPI (blue) and white arrows indicate the sperm flagellum in *Ccdc38*$^{+/+}$ and *Ccdc38*$^{-/-}$ mice. (C) Immunofluorescence analysis of Ac-TUBULIN (red) and PNA lectin (green) to identify sperm flagellum biogenesis. White arrows indicate short tails

were found from stage IV-V in *Ccdc38*$^{-/-}$ mice as compared with the control group. (D) Cross-sections of *Ccdc38*$^{-/-}$ sperm tails revealed the disorganization of axonemal microtubules and tail accessory structures. Red arrowheads indicate abnormal mitochondrial and the cytoplasm, blue arrowheads indicate the loss of outer dense fibers, the green arrowhead indicates the abnormal fibrous sheath, and the yellow arrowhead indicates the abnormal axoneme. Scale bars: 10 μm (A, B); 5 μm (C); 100 nm (D).

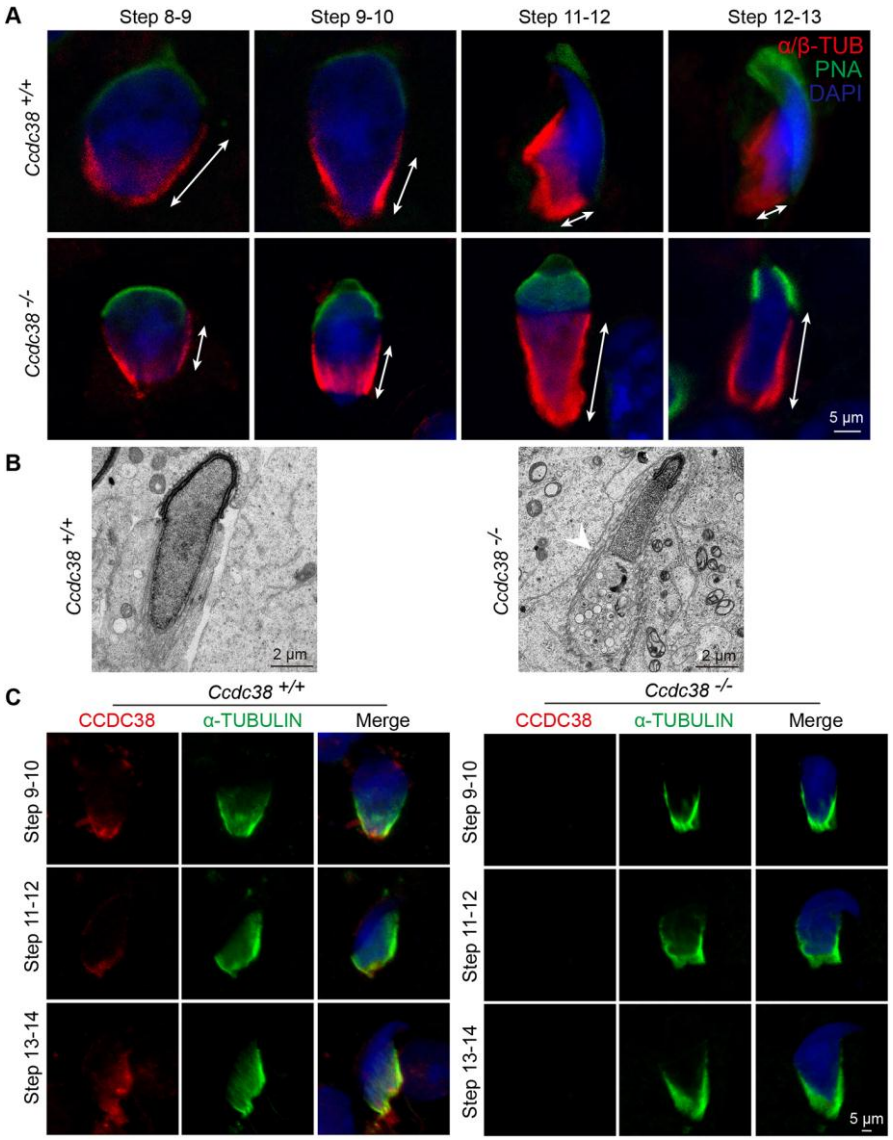

Fig. 6. The manchette is ectopically placed in *Ccdc38*$^{-/-}$ spermatids. (A) Abnormal manchette elongation in *Ccdc38*$^{-/-}$ spermatids. Spermatids from different manchette-containing steps were stained with α/β-TUBULIN antibody (red) and PNA lectin (green, acrosome marker) to visualize the manchette. *Ccdc38*$^{-/-}$ spermatids displayed abnormal elongation of the manchette. (B) TEM revealed that the manchette of elongating spermatids (steps 9-11) from *Ccdc38*$^{-/-}$ mice were ectopically placed. The white arrowhead indicates the abnormal manchette. (C) Localization of CCDC38 during different germ-cell stages. Immunofluorescence of CCDC38 and α-TUBULIN in developing germ cells. The manchette was stained with anti-α-TUBULIN antibody, and nuclei were stained with DAPI. Scale bars: 5 μm (A, C); 2 μm (B).

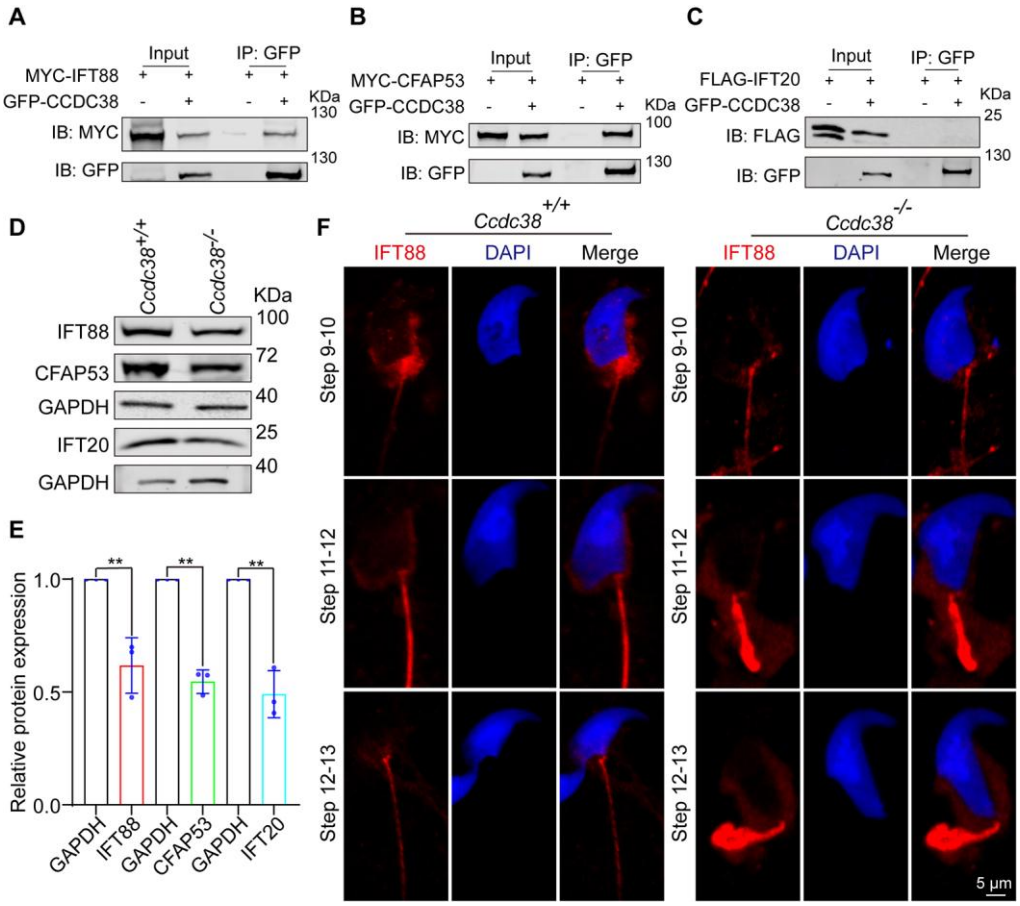

Fig. 7. CCDC38 interacts with IFT88. (A) CCDC38 interacted with IFT88. pCSII-MYC-IFT88 and pEGFP-C1-CCDC38 plasmids were transfected into HEK293T cells. Forty-eight hours after transfection, cells were collected for immunoprecipitation with anti-GFP antibody, and analyzed with anti-MYC or anti-GFP antibodies, respectively. (B) CCDC38 interacted with CFAP53. pCSII-MYC-CFAP53 and pEGFP-C1-CCDC38 plasmids were transfected into HEK293T cells. Forty-eight hours after transfection, cells were collected for immunoprecipitation with anti-GFP antibody, and analyzed with anti-MYC or anti-GFP antibodies, respectively. (C) CCDC38 couldn't interact with IFT20. pRK-FLAG-IFT20 and pEGFP-C1-CCDC38 plasmids were transfected into HEK293T cells. Forty-eight hours after transfection, cells were collected for immunoprecipitation with anti-GFP antibody, and analyzed with anti-FLAG or anti-GFP antibodies, respectively. (C) Western blotting analysis showed IFT88, CFAP53 and IFT20 protein levels in *Ccdc38*$^{+/+}$ and

Ccdc38$^{-/-}$ mice testis lysates. GAPDH served as a loading control. (D) Quantitative results of western blotting. $^{**}P < 0.01$. (E) Immunofluorescence of IFT88 (red) and DAPI (blue) in different-stage spermatids from *Ccdc38*$^{+/+}$ and *Ccdc38*$^{-/-}$ mice. Data are presented as the mean ± SD. Scale bars: 5 μm.

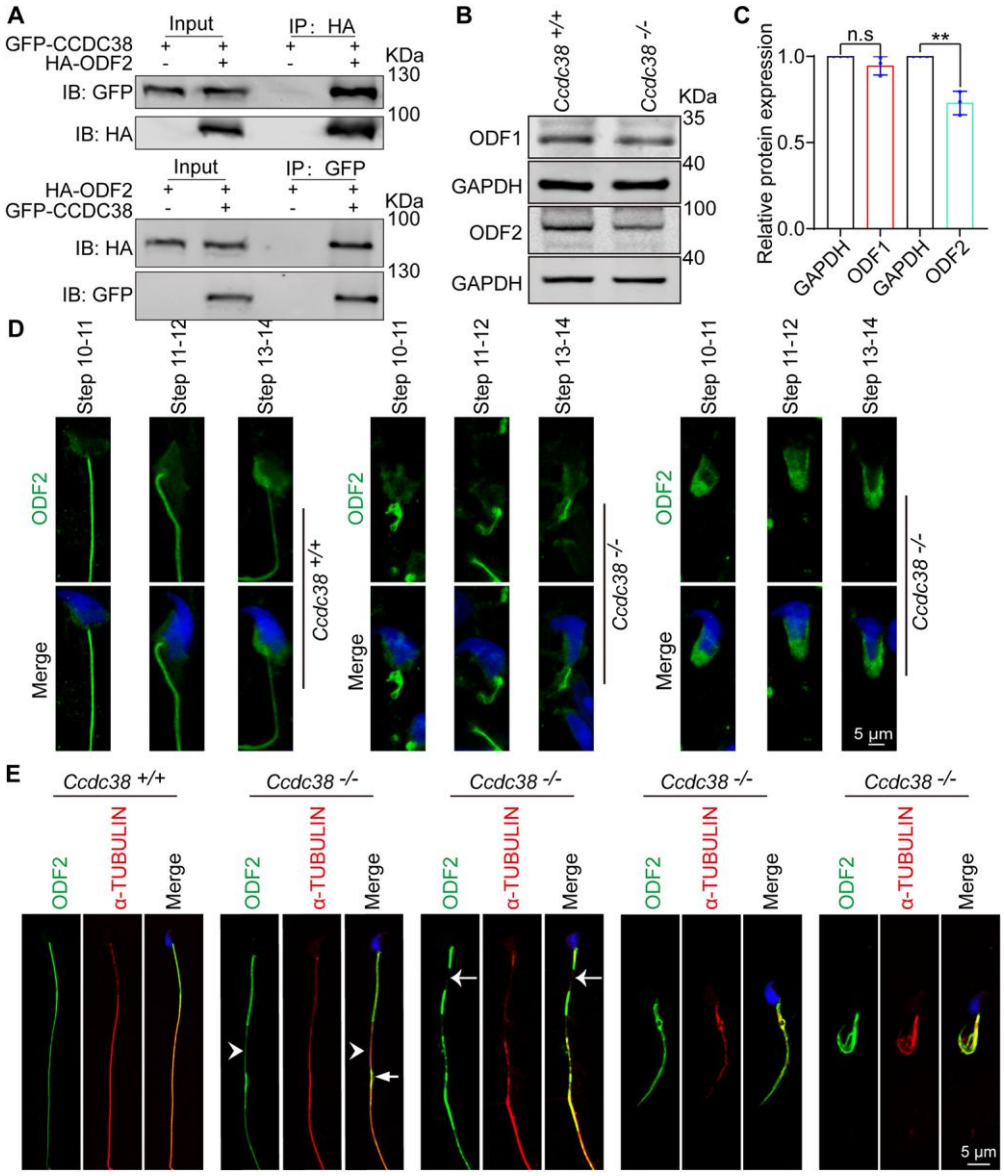

Fig 8. ODF transportation is impaired in *Ccdc*38 knockout spermatids. (A) CCDC38 interacted with ODF2. pCDNA-HA-ODF2 and pEGFP-C1-CCDC38 plasmids were transfected into HEK293T cells. Forty-eight hours after transfection, cells were collected for immunoprecipitation with anti-GFP or anti-HA antibodies, and then analyzed with anti-GFP or anti-HA antibodies, respectively. (B) Western blotting analysis to show ODF1 and ODF2 protein levels in *Ccdc38*$^{+/+}$ and *Ccdc38*$^{-/-}$ mice testis lysates. GAPDH served as a loading control. ODF2 protein levels were decreased. (C) Quantitative results of the western blot. $^{**}P < 0.01$. (D) The localization of ODF2 in testis germ cells. Testicular germ cells were stained with anti-

ODF2 antibody (green). ODF2 was localized in spermatid flagellum and the manchette of *Ccdc38*$^{-/-}$ or *Ccdc38*$^{+/+}$ germ cells. (E) Immunofluorescence of ODF2 (green) and α-TUBULIN (red) in spermatids from *Ccdc38*$^{+/+}$ and *Ccdc38*$^{-/-}$ mice. Nuclei were stained with DAPI (blue). Short white arrows indicate disordered axoneme, long white arrows indicate a discontinuous, punctiform short axoneme, while white arrowheads indicate a tenuous axoneme. Data are presented as the mean ± SD. Scale bars: 5 μm.

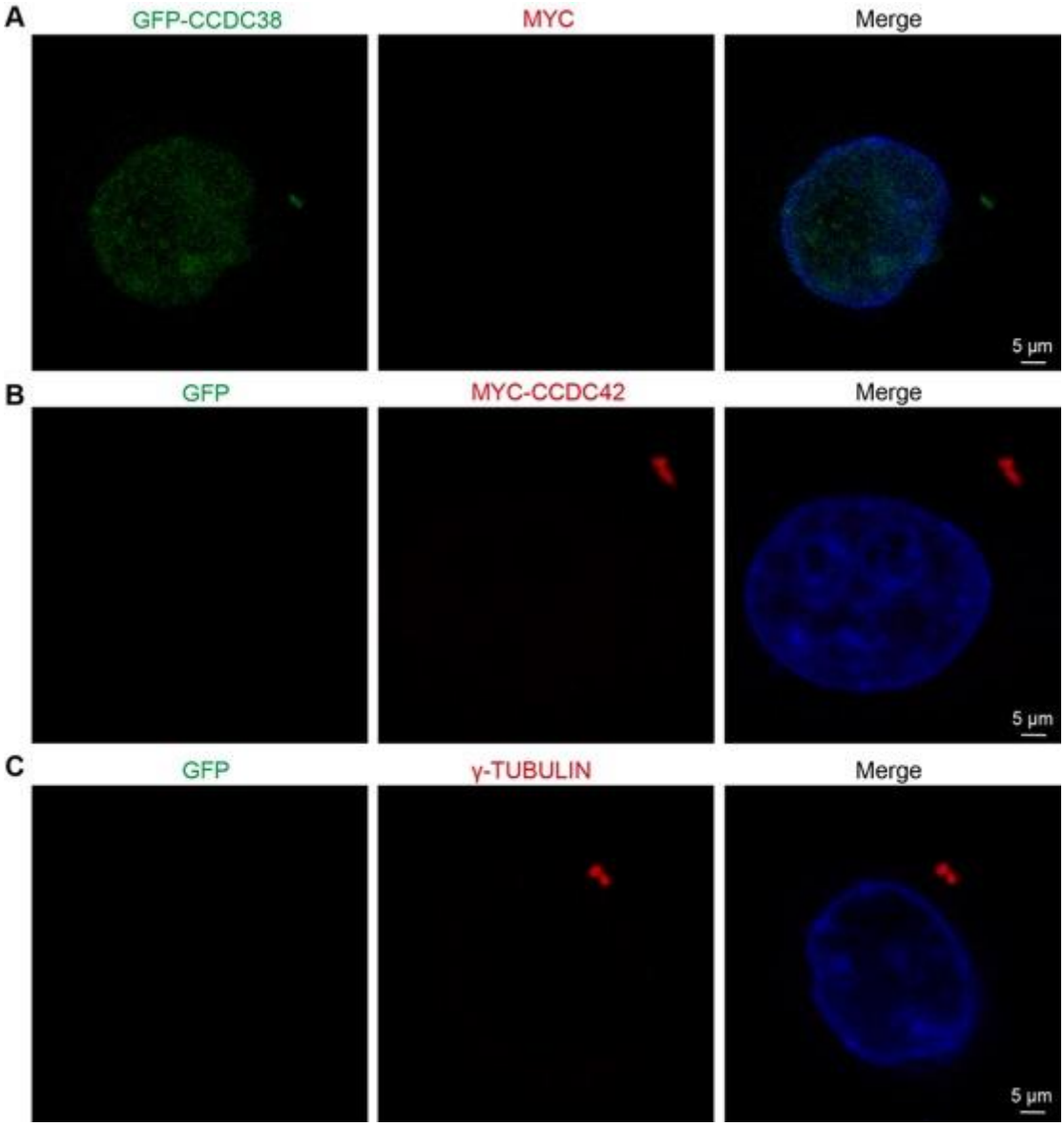

Fig. S1. Immunofluorescence analysis shows the localization of CCDC38 in somatic cells. (A-B) Immunofluorescence analysis using anti-GFP (green) and anti-MYC (red) antibodies was performed in Hela cells. Nuclei were stained with DAPI (blue). (C) Immunofluorescence analysis using anti-GFP (green) and anti-γ-TUBULIN (red) antibodies were performed in Hela cells. Nuclei were stained with DAPI (blue). Scale bars: 5 μm.

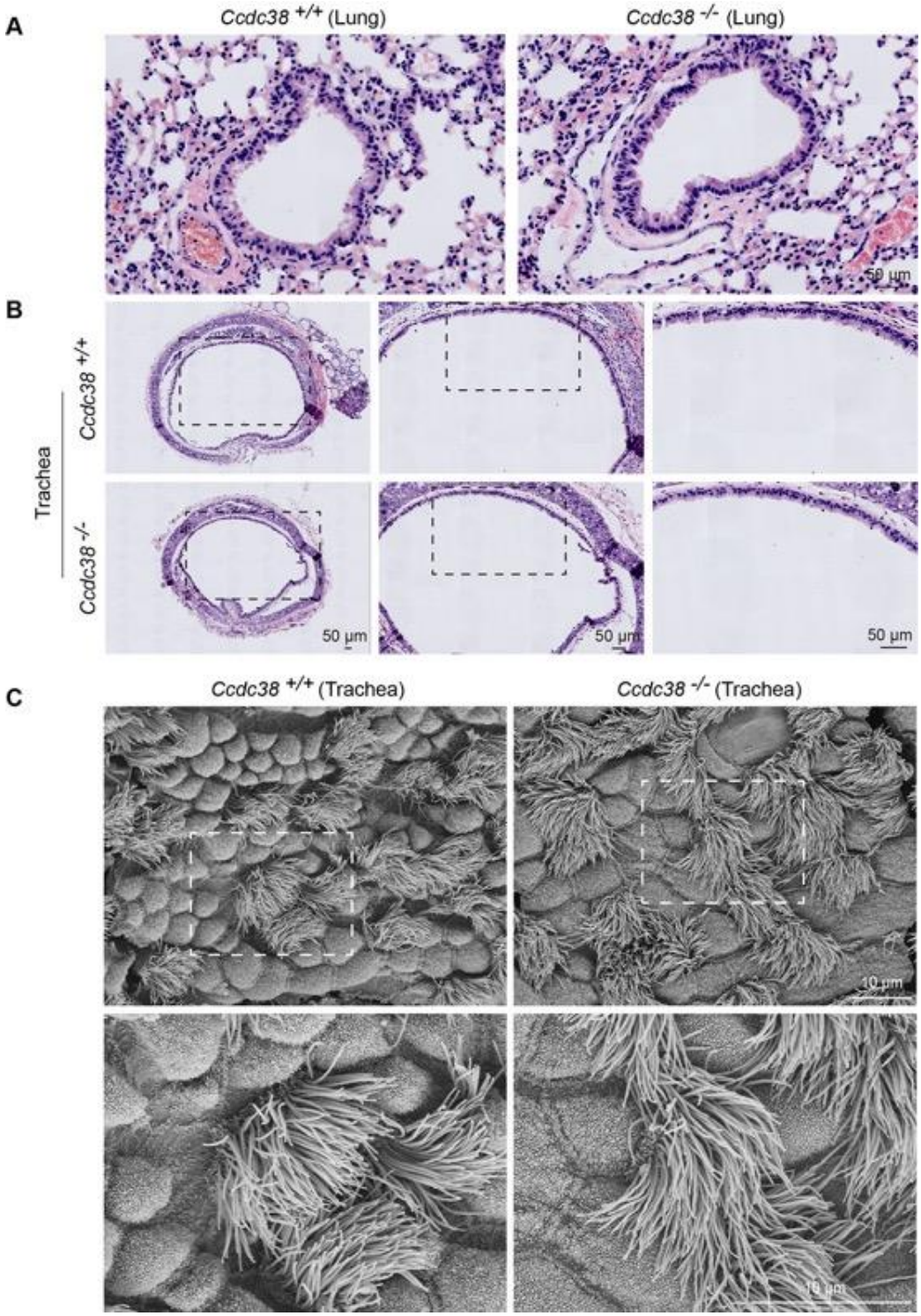

Fig. S2. Trachea cilia and lung cilia appear normal in *Ccdc38*$^{-/-}$ mice. (A) The histology of the lung from *Ccdc38*$^{+/+}$ and *Ccdc38*$^{-/-}$ mice. (B) The histology of the trachea from *Ccdc38*$^{+/+}$ and *Ccdc38*$^{-/-}$ mice. (C) Scanning electron micrography of *Ccdc38*$^{+/+}$ and *Ccdc38*$^{-/-}$ tracheal epithelium at low (upper) and high magnifications of the boxed areas (lower). Scale bars: 50 μm (A, B); 10 μm (C).

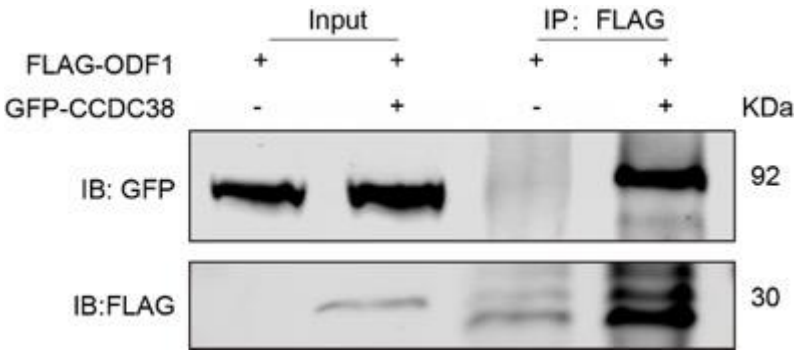

Fig. S3. CCDC38 can interact with ODF1. pRK-FLAG-ODF1 and pEGFP-C1-CCDC38 plasmids were transfected into HEK293T cells. Forty-eight hours after transfection, cells were collected for immunoprecipitation with anti-FLAG and analyzed with GFP or FLAG antibodies, respectively.